

Evolutions of self-assembled Bi₂O₃/LDHs nanostructures to mixtures of mixed oxides and their photocatalytic efficiency under UV and solar light

K. Katsumata^{*}, M. Puscasu^{**}, E. Seftel^{***}, E. F. Grosu^{**}, K. Ikeda^{*}, P. Cool^{***}
and G. Carja^{**}

^{*} Materials and Structures Laboratory, Tokyo Institute of Technology, 4259 Nagatsuta, Midori, Yokohama, 226-8503, Tokyo, Japan

^{**} Department of Chemical Engineering, Faculty of Chemical Engineering and Environmental Protection, Technical University “Gh. Asachi” of Iasi, Bd. Mangeron no.71, Iasi 700554, Romania, carja@uaic.ro

^{***} Laboratory of Adsorption and Catalysis, Department of Chemistry, University of Antwerpen (CDE), Universiteitsplein 1, 2610 Wilrijk, Antwerpen, Belgium

ABSTRACT

In this work we report self-assemblies of nanoparticles of Bi₂O₃ and layered double hydroxides (LDHs) obtained by exploiting the manifestation of the “structural memory effect” of ZnAILDH and ZnCrLDH anionic clay matrices in Bi(NO₃)₃ aqueous solutions. Controlled thermal treatment of Bi₂O₃/ZnAILDH and Bi₂O₃/ZnCrLDH self-assemblies gives rise to photoresponsive mixtures of mixed oxides, types Bi₂O₃/ZnO-ZnAl₂O₄ and Bi₂O₃/ZnO-ZnCr₂O₄, respectively. Powder X-ray diffraction (PXRD), X-ray photoelectron spectroscopy (XPS), high resolution transmission electron microscopy (TEM) and UV-Visible spectroscopy (UV-Vis) showed that the LDHs reconstruction in Bi(NO₃)₃ solutions gives rise to specific nanoarchitectonics characteristics in which small NPs of Bi₂O₃ (~5 nm) are highly dispersed on the larger NPs (~150 nm) of ZnAILDH and ZnCrLDH. UV-Vis analysis indicates the cooperative absorbance capabilities of the novel catalytic systems that were evaluated in the degradation process of phenol from aqueous solutions under solar and UV light.

Keywords: Bi₂O₃, LDHs self-assembled nanocomposites, solar irradiation, photocatalyst

1 INTRODUCTION

In recent years increasing attention is given on designing complex nanocomposites systems engineered to act as efficient photocatalysts; the unique nano size-dependent transport properties related to photons are able to establish specific photoresponsive functions that cannot be achieved by their bulk counterparts [1]. In this regard, manipulation of the photocatalytic properties by selective control of the catalyst nanoarchitectonics and by utilizing

the collective properties of nanoassembly systems is a continuous challenge [2]. Design of photocatalysts nanoarchitectonics refers not only to their simple construction as nanomaterials but also to ensemble different nanoscaled structural building units in designed and defined ways for creating complex formulations owning collective and synergic properties [3]. Layered double hydroxides (LDHs) are a class of anionic clays. An important property of LDHs is their structural “memory effect”; it refers to the structural reconstruction of the layered clay matrix when the metal mixed oxides, evolved after the calcination around 550°C, are exposed to the aqueous solutions containing anions [4]. Using the manifestation of the LDHs structural “memory effect” in the aqueous solutions of metal salts, we have recently reported a simple fabrication procedure of nanoparticles of metal oxides-LDHs (MexOy/LDHs) as self assemblies [5]. According to this procedure LDH matrix is able to rebuild its structure by using the anions of the solution as interlayer anions and also to adsorb the metal cations of the aqueous solution and organizing them as nanoparticles (NPs) of metal oxides on its surface [6, 7]. MexOy/LDHs self-enssembled composites with a large compositional diversity can be designed by modifying either the nature of the metal cations of the LDHs layers and/or the nature of the NPs of MexOy. NPs of Bi₂O₃ has attracted a great deal of attention in the last years [8]. Hence the joined functionalities of NPs of Bi₂O₃ and LDHs might give rise to unique photoresponsive characteristics.

Herein, we report for the first time the self - assemblies of NPs of Bi₂O₃ with the specific compositions of ZnAILDH and ZnCrLDH and their evolution, after the thermal treatment at 800°C to nanostructured mixtures of mixed oxides, types Bi₂O₃/ZnO-ZnAl₂O₄ and Bi₂O₃/ZnO-ZnCr₂O₄. The fabrication procedure of Bi₂O₃/LDHs is simple and cost-effective. It is based on the reconstruction of the LDH clays, due to the “structural memory” in the aqueous solution of Bi(NO₃)₃, at room temperature [6]. Results show that nanoarchitectonics of Bi₂O₃/LDHs and

the derived mixed oxides systems are active photocatalysts in the process of phenol photodegradation from aqueous solutions.

2 RESULTS AND DISCUSSIONS

2.1. XRD, TEM and XPS analyses

The crystalline structure of $\text{Bi}_2\text{O}_3/\text{ZnAlLDH}$ and $\text{Bi}_2\text{O}_3/\text{ZnCrLDH}$ - as reconstructed in Bi_2O_3 solution and after calcination at 800°C - was first characterized by XRD. Fig. 1A illustrates the characteristics of the obtained powder X-ray diffraction patterns of $\text{Bi}_2\text{O}_3/\text{ZnAlLDH}$ and $\text{Bi}_2\text{O}_3/\text{ZnCrLDH}$. It reveals that $\text{Bi}_2\text{O}_3/\text{ZnAlLDH}$ s consists of crystalline phases with reflections clearly assigned to the regular layered structure of hydrotalcite-like clay (ICDD file No. 22-700), in which a series of sharp and symmetric basal reflections of the $(00\ell, \ell = 3, 6, 9)$ planes and broad, less intense, reflections for the nonbasal $(01\ell, \ell = 2, 5, 8)$ planes are easily recognized [5].

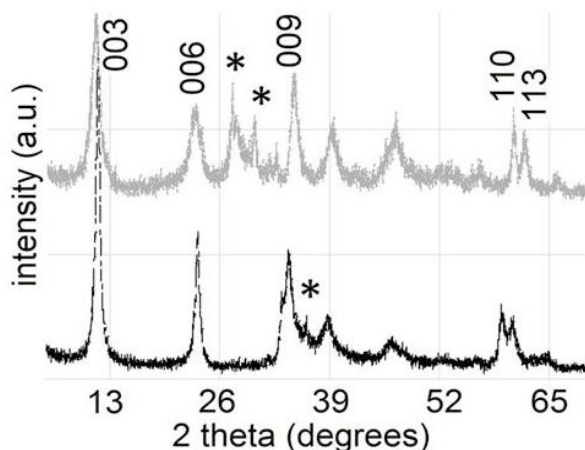


Fig. 1A. The XRD patterns of (-) $\text{Bi}_2\text{O}_3/\text{ZnAlLDH}$ and (-) $\text{Bi}_2\text{O}_3/\text{ZnCrLDH}$.

On the other hand, besides the reflections assigned to the regular layered structure of LDH some weaker reflections, (marked by *) in Fig. 1A), with positions which roughly coincide with those of mixed oxides that define the structure of the calcined LDHs can be also identified indicating that the structural reconstruction of the LDHs was not complete. Further, the structural characteristics of the mixtures of mixed oxides obtained after the calcination at 800°C of the as-synthesized and the reconstructed LDHs are shown in Fig. 1B for ZnAlLDH and Fig. 1C for ZnCrLDH , respectively. In Fig 1B some sets of diffraction peaks that can be indexed to hexagonal wurtzite ZnO (JCPDS file no 36-1451), ZnAl_2O_4 spinel (JCPDS file No. 5-0669) can be clearly identified while the new peaks observed at 2θ values $27.9, 33.7, 46.6,$ and 47.1° might correspond to $(121), (122), (041)$ and (104) diffraction planes of $\alpha\text{-Bi}_2\text{O}_3$ (JCPDS no. 71-2274). Hence, in this case, a mixture of $\alpha\text{-Bi}_2\text{O}_3/\text{ZnO-ZnAl}_2\text{O}_4$ was obtained. In

comparison the XRD pattern of $\text{Bi}_2\text{O}_3/\text{ZnCrLDH}$ calcined at 800°C indicates the formation of a mixture of mixed oxides, type $\alpha\text{-Bi}_2\text{O}_3/\text{ZnCr}_2\text{O}_4\text{-ZnO}$.

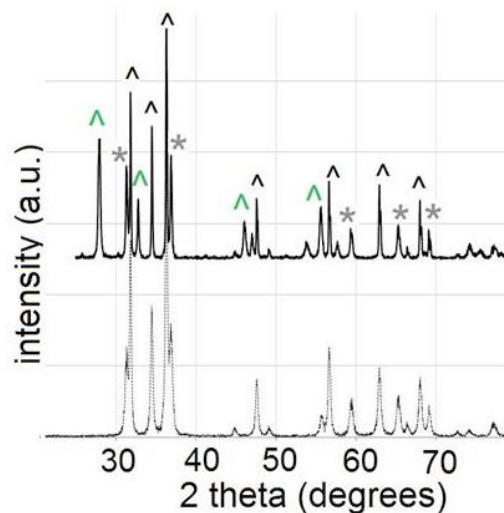


Fig. 1B. The XRD patterns of the mixed oxides derived from - $\text{Bi}_2\text{O}_3/\text{ZnAlLDH}$ and - ZnAlLDH after calcination at 800°C ; (\wedge) Bi_2O_3 , (\wedge) ZnO , (*) ZnAl_2O_4 .

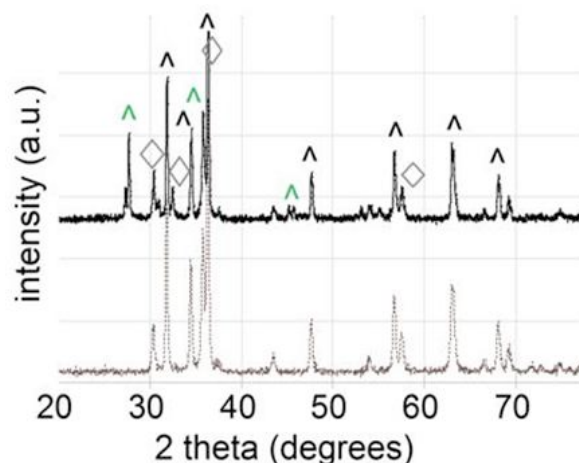


Fig. 1C. The XRD patterns of the mixed oxides derived from (-) $\text{Bi}_2\text{O}_3/\text{ZnCrLDH}$ and (-) ZnCrLDH after calcination at 800°C ; (\wedge) Bi_2O_3 , (\wedge) ZnO , (\diamond) ZnCr_2O_4 .

The detailed crystal structure and morphology was observed by TEM. Fig. 2A-D shows TEM as well as HRTEM images of $\text{Bi}_2\text{O}_3/\text{ZnAlLDH}$ and $\text{Bi}_2\text{O}_3/\text{ZnCrLDH}$. Fig. 2A illustrates that the reconstructed LDHs shows the conventional LDHs morphology consisting of aggregates of platelet-like particles with average sizes of ~ 150 nm. In the typical transmission electron microscopy (TEM) image (see Fig. 2B and 2D) very small NPs can be clearly observed as dark spots highly dispersed on the larger particle of the clay; the average size of the loaded NPs is 4.7 nm for

$\text{Bi}_2\text{O}_3/\text{ZnAlLDH}$ and 5.4 nm for $\text{Bi}_2\text{O}_3/\text{ZnCrLDH}$. The HRTEM image, (see Fig. 2C) indicates that the small NPs are highly crystalline with a well defined spacing of ca. 0.31 nm between adjacent lattice fringes, close to the d-spacing value of the (111) plane of $\alpha\text{-Bi}_2\text{O}_3$ [9].

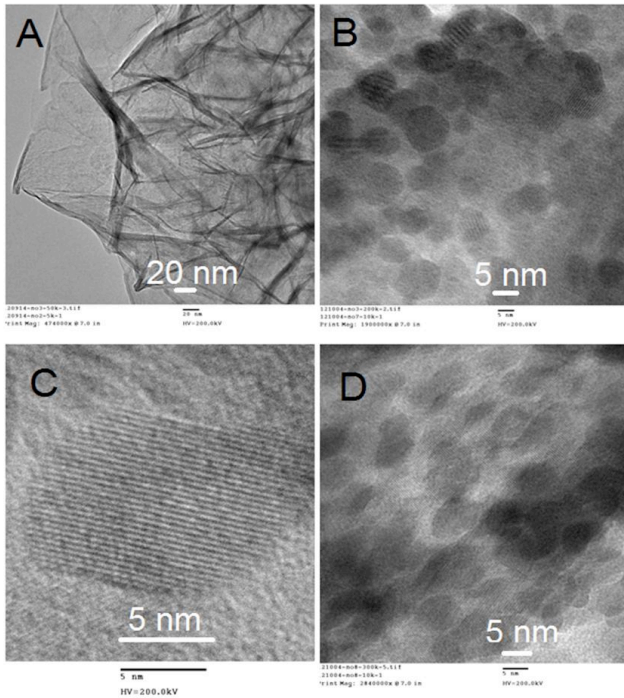


Fig. 2. The TEM and HRTEM images of $\text{Bi}_2\text{O}_3/\text{LDHs}$.

After calcination at 800°C the evolved mixed oxides presents different nano-sized features. Fig. 3 shows the TEM images of the mixed oxides $\text{Bi}_2\text{O}_3/\text{ZnO-ZnAl}_2\text{O}_4$ and $\alpha\text{-Bi}_2\text{O}_3/\text{ZnCr}_2\text{O}_4\text{-ZnO}$. It reveals that the nanoarchitectonic of the mixed oxides systems might be described by two types of nanoparticles with diameters equal of 9 and 12 nm, respectively. It is interesting to note that in the mixed oxides nanoparticles are interconnected each others revealing a heterojunction between the mixed oxides.

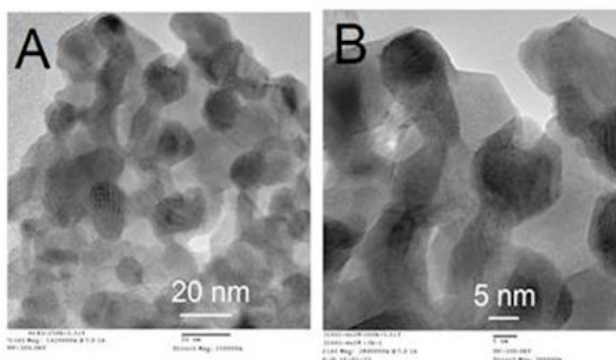


Fig. 3. The TEM images of (A) $\text{Bi}_2\text{O}_3/\text{ZnO-ZnAl}_2\text{O}_4$ and (B) $\text{Bi}_2\text{O}_3/\text{ZnCr}_2\text{O}_4\text{-ZnO}$.

XPS results further confirm the formation of $\text{Bi}_2\text{O}_3/\text{LDHs}$ self-assemblies and indicate that their similar Bi content (equal to $\sim 3\%$). For $\text{Bi}_2\text{O}_3/\text{ZnAlLDH}$ the survey EDX-XPS spectra is presented in Fig. 4 while the XPS spectra of

$\text{Bi}_2\text{O}_3/\text{ZnCrLDH}$ is given in Fig. 5. The analysis detected peaks from Bi, Zn, Al and O for $\text{Bi}_2\text{O}_3/\text{ZnAlLDH}$ while Bi, Zn, Cr, and O were identified in the surface elemental composition of $\text{Bi}_2\text{O}_3/\text{ZnCrLDH}$. These results indicate the joined surface composition of AuNPs and specific LDH clay matrix.

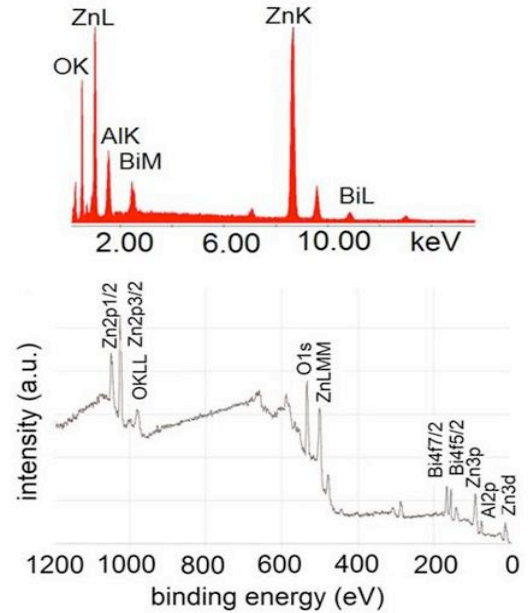


Fig. 4. High resolution XPS and EDX spectra of $\text{Bi}_2\text{O}_3/\text{ZnAlLDH}$.

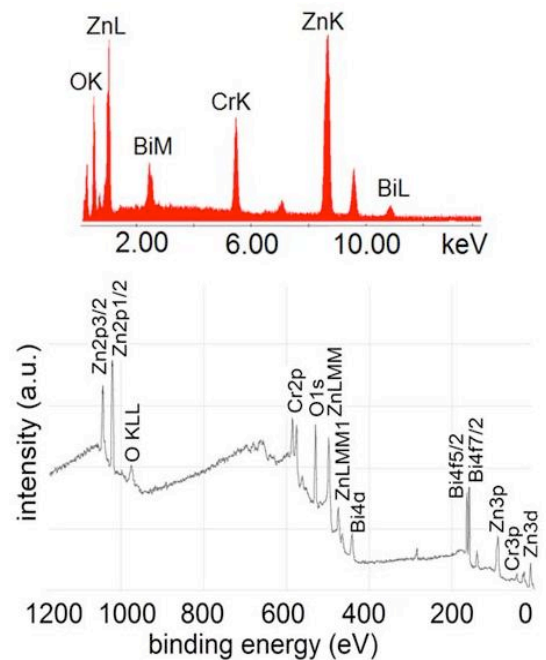


Fig. 5. High resolution XPS and EDX spectra of $\text{Bi}_2\text{O}_3/\text{ZnCrLDH}$.

2.2. Optical characteristics and photocatalytic properties

Fig. 6 displays the comparison of the room temperature UV-Vis absorption spectra of the studied catalysts. For all the samples the absorption in the UV region is defined by high intensities peaks that can be assigned to the optical responses of the LDHs and their derived mixed oxides.

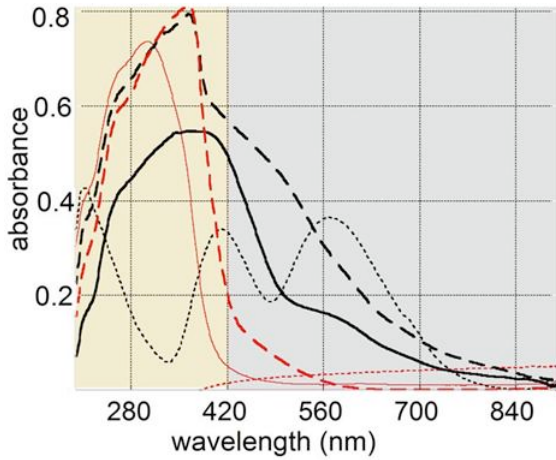


Fig. 6. The UV-Vis absorption spectra of: (-) $\text{Bi}_2\text{O}_3/\text{ZnAlLDH}$, (-) $\text{Bi}_2\text{O}_3/\text{ZnCrLDH}$, (---) $\text{Bi}_2\text{O}_3/\text{ZnO-ZnAl}_2\text{O}_4$ and (---) $\text{Bi}_2\text{O}_3/\text{ZnCr}_2\text{O}_4\text{-ZnO}$.

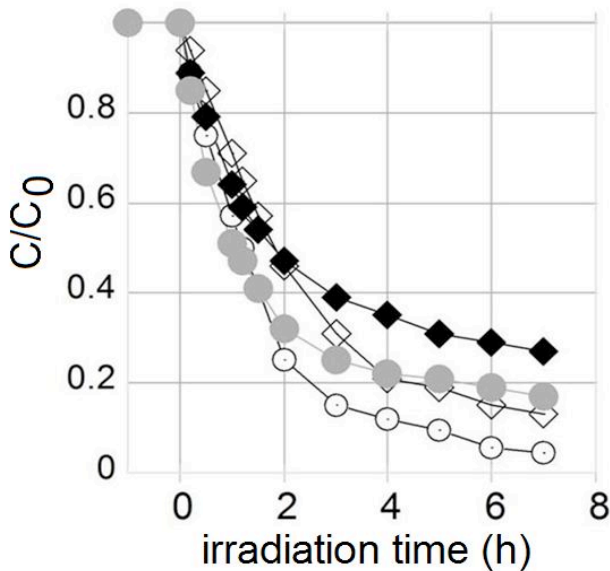


Fig. 7. Comparison of the photocatalytic efficiency of the catalysts during the photodegradation process of phenol over the entire range of wavelength: (●) $\text{Bi}_2\text{O}_3/\text{ZnCrLDH}$, (◆) $\text{Bi}_2\text{O}_3/\text{ZnAlLDH}$, (○) $\text{Bi}_2\text{O}_3/\text{ZnO-ZnAl}_2\text{O}_4$ (◇) $\text{Bi}_2\text{O}_3/\text{ZnCr}_2\text{O}_4\text{-ZnO}$.

One essential property relevant to the photocatalytic activity of a semiconductor is its energy band configuration. Tuning the energy band gap is a fundamental aspect of the

design and fabrication of photocatalysts. The energy band gap configuration will define the absorption of incident photons, the carriers and the redox capabilities of excited-state electrons and holes [11]. Thus, a classical Tauc approach is used to estimate the optical direct band gap (E_g) values of the samples. The obtained E_g values are 3.11 for $\text{Bi}_2\text{O}_3/\text{ZnO-ZnAl}_2\text{O}_4$ and 2.27 for $\text{Bi}_2\text{O}_3/\text{ZnCr}_2\text{O}_4\text{-ZnO}$. For the entire range of wavelength the photocatalytic efficiency of $\text{Bi}_2\text{O}_3/\text{LDHs}$ and the derived mixed oxides are compared in Figure 8. Controlled experiments indicate that that phenol pollutant does not degrade in the absence of photocatalyst. $\text{Bi}_2\text{O}_3/\text{ZnO-ZnAl}_2\text{O}_4$ shows the highest catalytic activity with almost complete degradation of the phenol after 6 h under irradiation while in the same conditions $\text{Bi}_2\text{O}_3/\text{ZnAlLDH}$ degrades only 82% of phenol.

REFERENCES

- [1] H. Tong, S. Ouyang, Y. Bi, N. Umezawa, M. Oshikiri and J. Ye, *Adv. Mater.*, 2012, 24, 229.
- [2] M. Grzelczak, J. Vermant, E. M. Furst and L. M. Liz-Marzaan, *ACS Nano*, 2010, 4, 3591.
- [3] K. Ariga, Q. Ji, M. J. McShane, Y. M. Lvov, A. Vinu and J. P. Hill, *Chem. Mater.*, 2012, 24, 728.
- [4] S. Mann, *Nature Mater.*, 2009, 8, 78.
- [5] S. Kawamura, M.C Puscasu., Y. Yoshida, Y. Izumi, G. Carja, *Applied Catalysis A: General*, 2014, in press.
- [6] G. Carja, M. Birsanu, K. Okada, H. Garcia, *Journal of Materials Chemistry*, 2013, 23, 6875-6883.
- [7] E.M. Seftel, M.C. Puscasu, M. Mertens, P. Cool, G. Carja, *Applied Catalysis B: Environmental*, 2015, 164, 251-260.
- [8] J. Prince, F. Tzompantzi, G. Mendoza-Damián, F. Hernández-Beltrán, J.S. Valente, *Applied Catalysis B: Environmental*, 2015, 163, 352-360.
- [9] G. Carja, L. Dartu, K. Okad, E. Fortunato, *Chemical Engineering Journal*, 2013, 222, 60-66.
- [10] S. Kannan, V. Rives and H. Knözinger, *J. Sol. St. Chem.*, 2004, 177, 319.
- [11] J. S. Valente, F. Tzompantzi, J. Prince, J. G.H. Cortez, R. Gomez, *Appl. Catal. B-Environ.*, 2009, 90, 330.

Acknowledgment: This work was supported in part by the Kazuchika Okura Memorial Foundation, “Planting Seeds for Research” program from Tokyo Institute of Technology, “Grant-in-Aid for Young Scientists (A; 25708037)” from Japan Society for the Promotion of Science (JSPS), and by the project “Development Base of Advanced Materials Development and Integration of Novel Structured Metallic and Inorganic” of the Ministry of Education, Culture, Sports, Science, and Technology (MEXT), Japan. This work was also supported by the grant of the Romanian National Authority for Scientific Research, CNCS-UEFISCDI, Project number PN-II-ID-PCE-75/2013.